# Synthesis and Characterization of a Bidirectional Photoswitchable Antagonist Toolbox for Real-Time GPCR Photopharmacology

Niels J. Hauwert, Tamara A. M. Mocking, Daniel Da Costa Pereira, Albert J. Kooistra, Lisa M. Wijnen, Gerda C. M. Vreeker, Eléonore W. E. Verweij, Albertus H. De Boer, Martine J. Smit, Chris De Graaf, Henry F. Vischer, Iwan J. P. de Esch, Maikel Wijtmans,* and Rob Leurs*

Division of Medicinal Chemistry, Amsterdam Institute for Molecules, Medicines and Systems, Faculty of Science, Vrije Universiteit Amsterdam, De Boelelaan 1108, 1081 HZ Amsterdam, The Netherlands

Ⓢ *Supporting Information*

ABSTRACT: Noninvasive methods to modulate G protein-coupled receptors (GPCRs) with temporal and spatial precision are in great demand. Photopharmacology uses photons to control *in situ* the biological properties of photoswitchable small-molecule ligands, which bodes well for chemical biological precision approaches. Integrating the light-switchable configurational properties of an azobenzene into the ligand core, we developed a bidirectional antagonist toolbox for an archetypical family A GPCR, the histamine H_3 receptor (H_3R). From 16 newly synthesized photoswitchable compounds, VUF14738 (**28**) and VUF14862 (**33**) were selected as they swiftly and reversibly photoisomerize and show over 10-fold increased or decreased H_3R binding affinities, respectively, upon illumination at 360 nm. Both ligands combine long thermal half-lives with fast and high photochemical *trans-/cis* conversion, allowing their use in real-time electrophysiology experiments with oocytes to confirm dynamic photomodulation of H_3R activation in repeated second-scale cycles. VUF14738 and VUF14862 are robust and fatigue-resistant photoswitchable GPCR antagonists suitable for spatiotemporal studies of H_3R signaling.
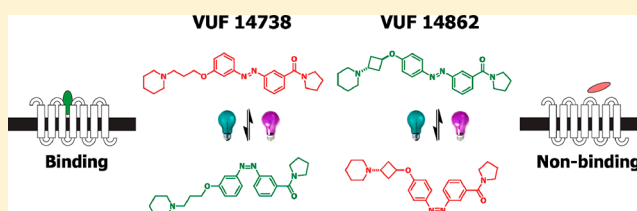
INTRODUCTION

Optical control of biological processes is one of the emerging fields in biomedicine due to its high spatiotemporal resolution.[1−5] Initially, optogenetics revolutionized the field with major breakthroughs in, e.g., the field of neuroscience.[3] Lately, the field of photopharmacology[1,2,5,6] has been providing a complementary framework allowing the use of photoswitchable ligand molecules to dynamically modulate native biological targets. In this framework, the photoinduced configuration of the ligand has either lower or higher affinity (directionality) than the "dark" configuration, providing a means to reversibly regulate the biological target with light. It has very recently been applied to, e.g., native membrane-bound ion channels[7−9] and G protein-coupled receptors (GPCRs).[10−14] Most GPCR examples have so far focused on single ligands typically incorporating a photosensitive group in the periphery of the GPCR ligands,[10−14] successfully giving reversible monodirectional photoswitches. In this work, we present a bidirectional photoswitchable GPCR antagonist toolbox, i.e., a set of ligands from the same scaffold amenable to switching in two directions, showing either a light-induced increase or decrease in GPCR affinity, by positioning the photoswitchable moiety in the core of the new ligands.

To this end, we used a prototypic family A GPCR, the histamine H_3 receptor (H_3R). The H_3R is expressed mainly in the central nervous system (CNS) and involved in a variety of CNS processes.[15−17] Recently, the first H_3R antagonist (pitolisant, Wakix) has been approved for the treatment of narcolepsy.[18] The medicinal chemistry of small-molecule H_3R ligands is well-developed[19,20] and provides interesting chemical opportunities to incorporate photoswitchable groups in order to obtain photoswitchable H_3R antagonists. The general H_3R antagonist pharmacophore includes a positively charged amine group,[21] which is considered to interact with either the amino acid residues $D114^{3.32}$ or $E206^{5.46}$ in the transmembrane part of the H_3R protein.[19,22,23] A linker, usually an alkyl ether, allows the ligand to make a slight kink toward the bottom of the orthosteric H_3R binding site. The ether oxygen atom is connected to an aromatic core (e.g., phenyl, naphthyl, and many others[19,20]), which allows for $\pi-\pi$ stacking interactions with aromatic H_3R residues, like the $Y115^{3.33}$, $Y374^{6.51}$, and $F398^{7.39}$ residues.[24−26] The aromatic core can be further substituted with a variety of groups including lipophilic groups, hydrogen bond acceptors, and basic and acidic moieties.[27] Various photoswitchable moieties were evaluated for replacement of the H_3R antagonist aromatic core[5] and the photoisomerizable azobenzene moiety was deemed the best fit because of the narrow, flat, and elongated aromatic nature of its *trans* isomer. Although a naphthalene moiety has not been coined as an "azostere",[1] our design started from a naphthalene-containing H_3R antagonist (**1**) developed by Roche et al.,[28] which matches the previously mentioned pharmacophore criteria. We postulated that, due to the relatively small nature
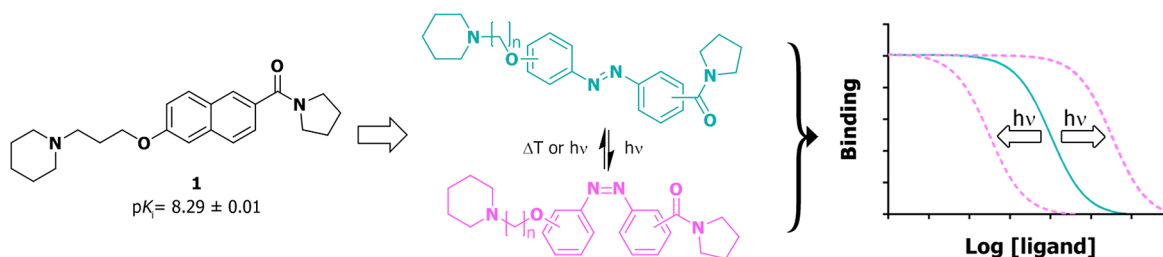
Figure 1. General design and concept of bidirectional photoswitchable H$_3$R antagonists. In this SAR study, the azobenzene moiety is incorporated in the core of compound **1** to give a series of differently substituted *trans* isomers (cyan). Illumination leads to their corresponding *cis* isomers (magenta). Within this study, we aimed to discover photoswitchable H$_3$R antagonists that show at least a 10-fold increase or decrease in GPCR affinity upon illumination.

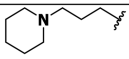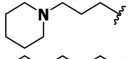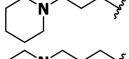**Scheme 1. General Synthetic Scheme for Photoswitchable H$_3$R Antagonists**[a]
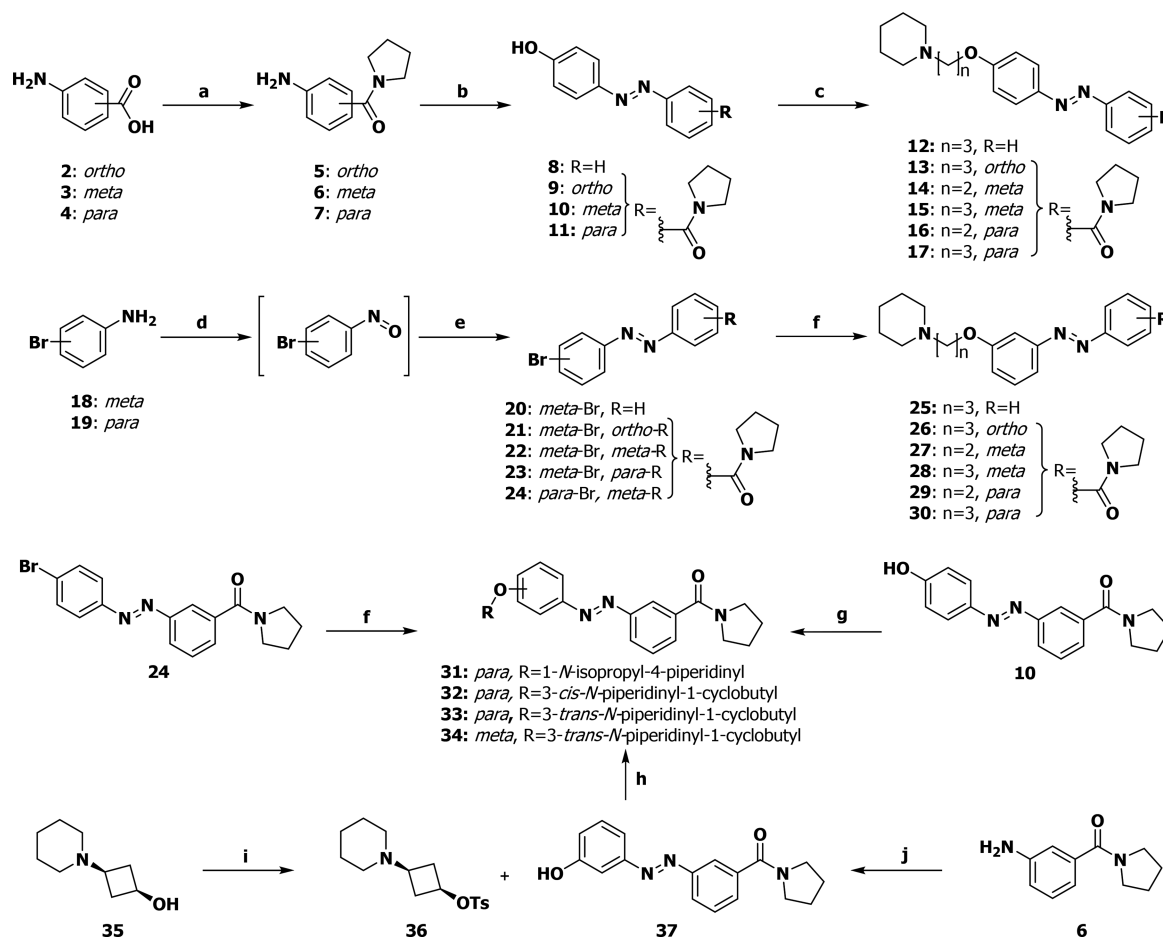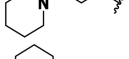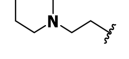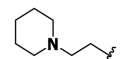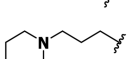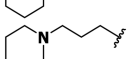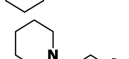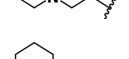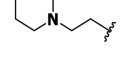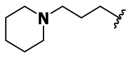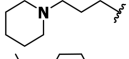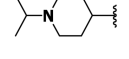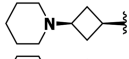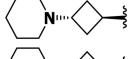
[a]Reagents and conditions: (a) pyrrolidine, EDCI·HCl, DIPEA, HOBt·H$_2$O, DMF, rt, 16 h, 57−95%; (b) (I) NaNO$_2$, 1 M aq HCl, 0 °C, 5 min; (II) phenol, aq NaOH, rt, 30 min; (III) 1 M aq HCl, aq satd NH$_4$Cl, rt, 10 min, 30−81%; (c) NaI, K$_2$CO$_3$, Pip-(CH$_2$)$_n$-Cl·HCl, DMF, 130 °C, 16 h, 31−76%; (d) Oxone, H$_2$O/DCM 4:1, rt, 3 h; (e) R-Ar-NH$_2$, AcOH/DCM 1:1, rt, 16 h, 30−76% (over two steps); (f) R-OH, RockPhos, [PdCl(C$_3$H$_5$)]$_2$, Cs$_2$CO$_3$, PhMe, 90 °C, 23 h, 12−47%; (g) R-OH, DEAD, PPh$_3$, THF, 0 °C→ rt, 18 h, 33−73%; (h) 1-methylimidazole, 4-MePhSO$_2$Cl, DCM, rt, 48 h, 43%; (i) (I) Oxone, H$_2$O/DCM 4:1, rt, 6 h; (II) 3-OTBMDS-aniline, AcOH, rt, 16 h; (III) TBAF, THF, 0 °C, 10 min, 13%; (j) (I) NaH, DMF, rt, 30 min; (II) **36**, 90 °C, 16 h, 59%; Pip = 1-piperidino.

of the naphthalene core, additional room for $\pi-\pi$ stacking interactions is present in the hydrophobic part of the H$_3$R binding site, allowing incorporation of the azobenzene photoswitch in the core of the H$_3$R scaffold (Figure 1) itself rather than in the periphery, as most often observed for GPCR photoligands.

In this paper, we show how this core-centered strategy led to the new H$_3$R antagonists VUF14738 and VUF14862 that represent a bidirectional set of robust and fatigue-resistant

photoswitchable GPCR antagonists and are unique assets to further detail H$_3$R pharmacology. We envision that these ligands are useful molecular tools for, e.g., probing H$_3$R-mediated responses in physiology in a similar fashion as stereoisomers like R- and S-α-methylhistamine,[29,30] but having control of H$_3$R affinity using an external trigger. Moreover, in view of the importance of the H$_3$R in various brain functions,[17,31] spatiotemporal photopharmacology approaches will bring new experimental options (next to optogenetics) in

Table 1. Structure−photochemistry Relationship of the Photoswitchable Azobenzene-Derived H$_3$R ligands

Compound Number	Scaffold	R	Amide position	λ_{max} $trans^a$ (nm)	λ_{max} cis^a (nm)	t½ @ 20 °C (days)^b	PSS^c ± SEM (area % cis)
12	A		-^{d}	344	432	11.2	96.6 ± 0.33
25	B		-^{d}	317	430	52.2	93.2 ± 0.29
17	A		4	352	435	9.52	88.2 ± 2.5
30	B		4	323	431	29.3	88.9 ± 1.3
16	A		4	349	434	0.23	86.6 ± 2.5
29	B		4	324	429	48.8	91.3 ± 1.4
15	A		3	347	432	26.5	95.4 ± 0.50
28	B		3	318	427	122	86.8 ± 0.63
14	A		3	345	431	0.69	90.6 ± 0.77
27	B		3	318	425	248	89.3 ± 0.50
13	A		2	351	430	10.9	88.9 ± 2.2
26	B		2	321	428	48.8	88.4 ± 1.8
31	A		3	346	434	33.5	90.5 ± 1.3
32	A		3	346	431	27.0	96.8 ± 0.21
33	A		3	346	432	29.2	94.6 ± 1.8
34	B		3	317	425	161	89.3 ± 0.40

^{a}Determined at 25 μM in 50 mM Tris-HCl pH 7.4 buffer + 1% DMSO-d_6. ^{b}Thermal relaxation half-life times were determined according to the method of Priimagi et al.[34] Arrhenius plots are available in Figure S1 ^{c}Photostationary state area percentages after illumination with 360 ± 20 nm at 1 mM in DMSO-d_6 and as determined by LC−MS analysis at 254 nm. ^{d}Unsubstituted phenyl moiety.

order to delineate the importance of local neuronal circuits in H$_3$R pharmacology.

■ RESULTS AND DISCUSSION

Synthesis and Photochemical Characterization of Azobenzene-Derived H$_3$ Ligands. Three synthesis routes were developed which allowed for great versatility in the substitution patterns of the azobenzene moiety (Scheme 1). A set of anilines was obtained by an amide coupling from **2**−**4** to **5**−**7**. The anilines underwent diazotization followed by a quench with phenol to afford **8**−**11** and Williamson ether synthesis to yield the *para*-ether-substituted H$_3$R photoswitchable ligands **12**−**17**.

The second route was designed to overcome the undesired *para*-selectivity in the diazotization and comprises oxidation of aniline **18** and **19** to a nitroso intermediate, condensation with an aniline to furnish **20**−**24** and a Pd/RockPhos-catalyzed ether synthesis[32] to yield *meta*-ether substituted ligands **25**−**30**. For the synthesis of constrained ligands, either a Mitsunobu reaction (for **31** and **33**) or a Pd/RockPhos-catalyzed ether synthesis[32] (for **32**) was employed instead of the Williamson ether synthesis. The Mitsunobu approach was unable to yield **34**, and instead, a tosylate-displacement strategy through intermediacy of **35**−**37** was used for this compound.[33]

We first investigated the photoisomerization of all final compounds as well as their thermal relaxation at 20 °C as determined by the method of Priimagi et al.[34] (Table 1, Figure
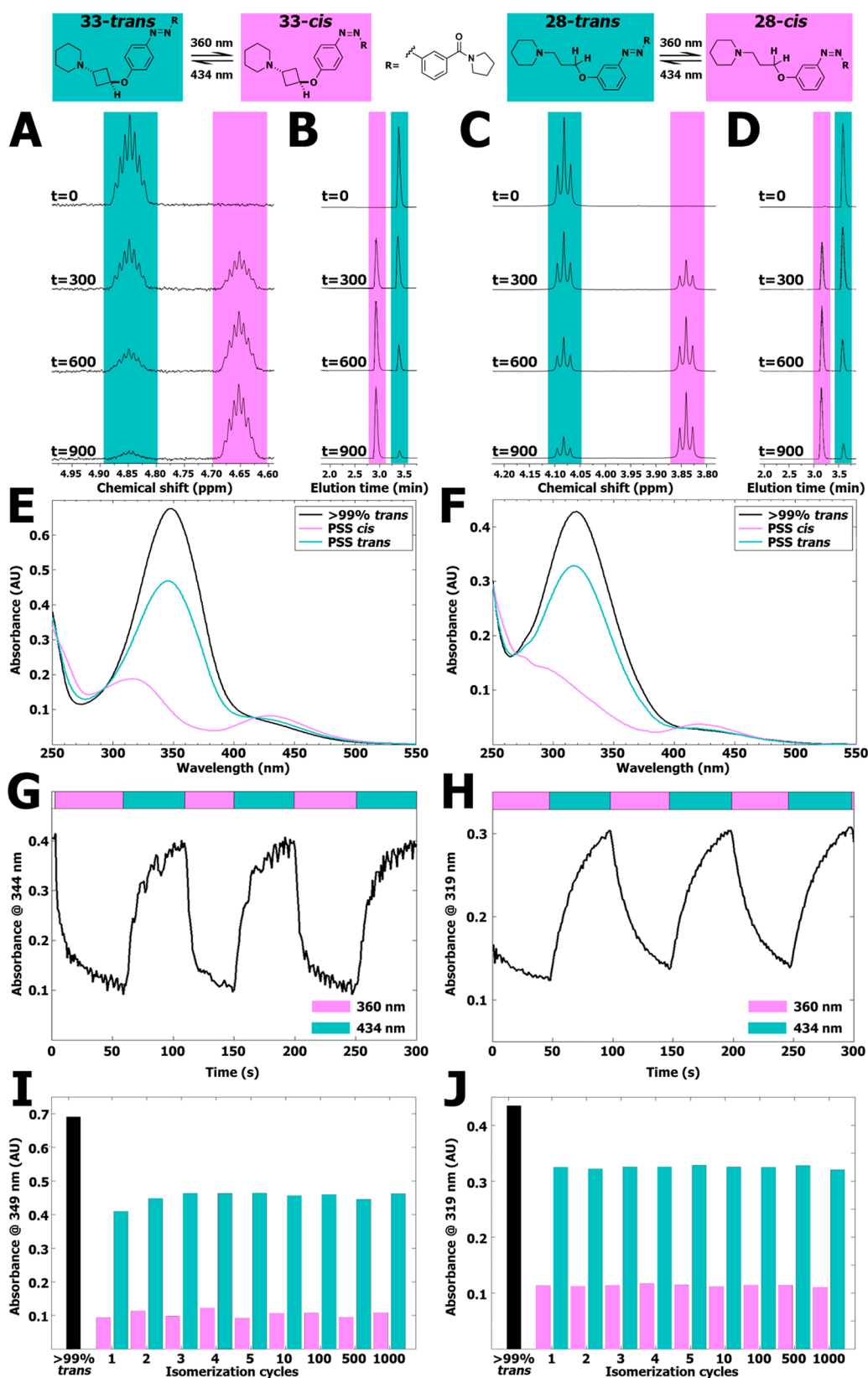
Figure 2. (A) Representative part of ^{1}H NMR spectra of 10 mM of compound **33** in DMSO-d_6 illuminated at 360 ± 20 nm displayed at various time points (seconds). The presented peak belongs to the hydrogen atom explicitly drawn in the structure shown above the spectrum. Full ^{1}H NMR spectra are available in Figure S18. (B) Representative part of LC−MS chromatograms belonging to the illuminated NMR samples shown in Figure 2A. The full chromatograms are available in Figure S19. (C) Representative part of ^{1}H NMR spectra of 10 mM of compound **28** in DMSO-d_6 illuminated at 360 ± 20 nm displayed at various time points (seconds). The presented peak belongs to the hydrogen atom explicitly drawn in the structure shown above the spectrum. Full ^{1}H NMR spectra are available in Figure S20. (D) Representative part of LC−MS chromatograms belonging to the illuminated NMR samples shown in Figure 2C. The full chromatograms are available in Figure S21. (E) UV−vis spectra of 25 μM

Figure 2. continued

of compound **33** (*trans*) in 50 mM Tris−HCl pH 7.4 buffer containing 1% DMSO-d_6. PSS *cis* represents a sample which has been illuminated for 300 s using 360 ± 20 nm light. PSS *trans* represents subsequent illumination for 300 s using 434 ± 9 nm. (F) UV−vis spectra of 25 μM of compound **28** (*trans*) in 50 mM Tris−HCl pH 7.4 buffer containing 1% DMSO-d_6. PSS *cis* represents a sample which has been illuminated for 300 s using 360 ± 20 nm. PSS *trans* represents subsequent illumination for 300 s using 434 ± 9 nm. (G) Absorbance at 344 nm of 25 μM of compound **33** in 50 mM Tris−HCl pH 7.4 buffer +1% DMSO-d_6. UV−vis spectra were obtained with 1 s intervals under alternating illumination with 360 ± 20 nm and 434 ± 9 nm perpendicular to the light source of the UV−vis spectrometer. (H) Absorbance at 319 nm of 25 μM of compound **28** in 50 mM Tris−HCl pH 7.4 buffer +1% DMSO-d_6. UV−vis spectra were obtained with 1 s intervals under alternating illumination with 360 ± 20 nm and 434 ± 9 nm perpendicular to the light source of the UV−vis spectrometer. (I) Repeated isomerization cycles of 25 μM of compound **33** in a pH 7.4 buffer containing 15 mM HEPES, 64 mM NaCl, 25 mM KCl, 0.4 mM CaCl₂, and 0.8 mM MgCl₂ containing 1% DMSO-d_6 analyzed at 349 nm. PSS *cis* was obtained by using illuminations for 20 s at 360 ± 20 nm. PSS *trans* was obtained by using illuminations for 20 s at 434 ± 9 nm. An extended figure is available in Figure S16. (J) Repeated isomerization cycles of 25 μM of compound **28** in a pH 7.4 buffer containing 15 mM HEPES, 64 mM NaCl, 25 mM KCl, 0.4 mM CaCl₂, and 0.8 mM MgCl₂ containing 1% DMSO-d_6 analyzed at 319 nm. PSS *cis* was obtained by using illuminations for 20 s at 360 ± 20 nm. PSS *trans* was obtained by using illuminations for 20 s at 434 ± 9 nm. An extended figure is available in Figure S17.

S1). Clear trends in the photochemistry could be deduced. It was observed that *para*-ether derivatives (scaffold A) have a distinctly higher λ_{max} for the $\pi−\pi^*$ transition of the *trans* isomers than *meta*-ether derivatives (scaffold B). This trend can be explained due to a better "push−pull" profile in the electron density of scaffold A, which is known to red shift the λ_{max} of electronic transitions.[35,36] It was found that upon continuous illumination at 10 mM in DMSO-d_6 with 360 ± 20 nm light a photostationary state (PSS) containing over 85% *cis* isomer (LC area at 254 nm) could be obtained for all compounds, with several ligands showing a PSS containing more than 95% *cis* isomer.

Various trends can be observed regarding the thermal relaxation half-lives of the compounds. In line with the literature, we observed a 3- to 5-fold difference in thermal relaxation half-life between the *para*-ethers (**12, 13, 15, 17**) and their respective *meta*-ether (**25, 26, 28, 30**) analogues having a propylpiperidine side chain.[37] Such an effect can be attributed to increased conjugation in the *para* derivatives.[38] In the series of ethylpiperidine analogues (**14** versus **27**, **16** versus **29**), this effect of *para*- versus *meta*-ether substitution is even more pronounced, increasing the differences in thermal relaxation half-life to 360- and 212-fold, respectively. The propyl, cyclobutyl, and 4-piperidinyl spacers appear to have a comparable influence on the thermal relaxation half-lives (compare **15** versus **31−33** and **15/28** versus **33/34**). If the amide group is placed at the *ortho* (**13, 26**) or *para* position (**17, 30**) the thermal relaxation half-life is comparable to its nonsubstituted counterpart (**12, 25**). However, having the amide in the *meta* position as in **15/28** yields a modest increase in thermal relaxation half-life.[39]

Compounds **28** and **33** were selected for further photochemical characterization based on their favorable pharmacological characteristics (vide infra). The thermal relaxation half-life times for these compounds in 50 mM Tris−HCl pH 7.4 buffer at room temperature were also directly determined, resulting in half-lives of 114 days for compound **28** (Figure S2) and 26 days for compound **33** (Figure S3). These long thermal relaxation half-lives are similar to the values obtained from the Arrhenius plots at 20 °C and uniquely allowed for a thorough analysis of the photoswitching and relaxation process by ^{1}H NMR spectroscopy in conjunction with LC−MS chromatography and UV−vis spectroscopy. We first investigated isomerization of **28** and **33** at 10 mM in DMSO-d_6 by monitoring both ^{1}H NMR and LC−MS profiles in time. While multiple ^{1}H NMR signals change upon photoswitching, the signals for the CH or CH₂ group adjacent to the ether O atom provided a clearly resolved signal for quantification (Figure 2A,C). For

both **28** and **33** the percentages of isomerization as analyzed by ^{1}H NMR spectroscopy and LC−MS analysis at 254 nm (Figure 2B,D) are comparable yet slightly different, reflecting most likely some differences in ε values of the *trans* and *cis* isomers (Table S1). Despite these minor differences, LC−MS was subsequently used as a routine analysis in view of the higher throughput.

Next, the photoisomerization rate was investigated at 25 μM in 50 mM Tris−HCl pH 7.4 buffer supplemented with 1% DMSO-d_6 using UV−vis spectroscopy (Figure 2E,F). Rapid photoisomerization was observed for both compounds during illuminations at both 360 ± 20 nm and 434 ± 9 nm to obtain high amounts of *cis* isomer or considerable amounts of *trans* isomer, respectively (Figures S4−S6 and S10−S12). After 30 s of illumination, isomerization of both key compounds had reached isomerization percentages within 5% of their PSS. Thus, illuminating for 300 s was always sufficient to reach PSS. Arguably due to both solvent and concentration effects,[36,40,41] the measured isomerization rates are considerably higher in the experiments performed at 25 μM in buffer, compared to the measurements at 10 mM in DMSO-d_6 of the two H₃R ligands.

We subsequently studied the real-time isomerization behavior of both compounds at a concentration of 25 μM in 50 mM Tris−HCl pH 7.4 buffer supplemented with 1% DMSO-d_6 using a setup which allowed the illumination perpendicular to the path of the UV−vis spectrometer light source. Under these conditions, we determined a photoisomerization half-life for **33** of 4 ± 0.2 s under illumination with 360 ± 20 nm and 8 ± 0.6 s under illumination with 434 ± 9 nm (Figure 2G). For **28**, the values were found to be 16 ± 0.9 s under illumination at 360 ± 20 nm and 11 ± 0.3 s under illumination at 434 ± 9 nm (Figure 2H).

Both photoswitchable compounds proved to be very photostable. Even after 48 h of illumination at 360 ± 20 nm with an intensity of 0.77 mW/mm², no apparent photodegradation was visible in both ^{1}H NMR and LC−MS analyses of **28** and **33**. To exemplify the resistance to fatigue of **28** and **33**, over 1000 isomerization cycles switching between illumination at 360 ± 20 and 434 ± 9 nm with 20 s intervals were executed. The absorbance at λ_{max} of the $\pi−\pi^*$ transition of the *trans* isomer did not alter considerably (Figure 2I,J and Figures S16 and S17), indicating that both key photoswitches are highly resistant to photobleaching.

Photopharmacological Characterization. Because of their long thermal relaxation half-lives, the newly synthesized photoswitchable GPCR ligands are uniquely compatible with competition radioligand-binding experiments. All new azoben-

**Table 2. Affinity for the Human H₃R of Photoswitchable Azobenzene-Derived H₃R Ligands**

Compound number	Scaffold	R	Amide position	PSS[a] ± SEM (area % *cis*)	pK_i *trans* ± SEM[b]	pK_i at PSS[a] ± SEM[b]	pK_i shift[c]	n
Histamine			-	-	7.89 ± 0.05	-	-	12
1			-	-	8.29 ± 0.01	-	-	3
12	A		-[d]	96.6 ± 0.33	7.33 ± 0.11	8.06 ± 0.06	0.74	5
25	B		-[d]	93.2 ± 0.29	6.42 ± 0.11[e]	7.04 ± 0.09	0.62	6
17	A		4	88.2 ± 2.5	7.96 ± 0.06	7.36 ± 0.02	−0.59	3
30	B		4	88.9 ± 1.3	6.01 ± 0.13	6.69 ± 0.15	0.68	6
16	A		4	86.6 ± 2.5	6.92 ± 0.12	6.56 ± 0.06	−0.36	5
29	B		4	91.3 ± 1.4	6.24 ± 0.02	5.96 ± 0.06	−0.28	3
15	A		3	95.4 ± 0.50	7.90 ± 0.07	7.26 ± 0.08	−0.63	5
28	B		3	86.8 ± 0.63	6.19 ± 0.11	7.32 ± 0.04	1.13	3
14	A		3	90.6 ± 0.77	6.16 ± 0.06	5.85 ± 0.14	−0.30	4
27	B		3	89.3 ± 0.50	6.19 ± 0.02	6.38 ± 0.01	0.19	4
13	A		2	88.9 ± 2.2	7.97 ± 0.13	7.55 ± 0.10	−0.41	4
26	B		2	88.4 ± 1.8	7.29 ± 0.08	7.09 ± 0.05	−0.19	4
31	A		3	90.5 ± 1.3	8.39 ± 0.09	7.40 ± 0.15	−0.98	5
32	A		3	96.8 ± 0.21	7.10 ± 0.12	6.48 ± 0.03	−0.62	3
33	A		3	94.6 ± 1.8	8.76 ± 0.09	7.71 ± 0.09	−1.05	4
34	B		3	89.3 ± 0.40	7.25 ± 0.04	7.15 ± 0.07	-0.10	4

[a]Photostationary state area percentages after illumination with 360 ± 20 nm at 1 mM in DMSO-d_6 and as determined by LCMS analysis at 254 nm. [b]Measured by displacement of [³H]-N^{α}-methylhistamine on HEK293T cell homogenates transiently expressing the H₃R. [c]Defined as pK_i PSS *cis* − pK_i *trans*. [d]Unsubstituted phenyl. [e]*Trans* sample contained 3.9 area % *cis* compound.

zene-derived H₃R ligands, either illuminated using 360 ± 20 nm to PSS (as determined by LC−MS) or kept in the dark, were evaluated for their affinity for the human H₃R by a [³H]-N^{α}-methylhistamine competition binding experiments performed in the dark. Both histamine and, as previously reported,[28] the parent naphthalene compound **1** potently displace [³H]-N^{α}-methylhistamine binding to membranes overexpressing the H₃R (Table 2), and their affinity values

were not affected by illumination of the compound solutions at 360 ± 20 nm (data not shown). Replacement of the naphthalene core of **1** with the azobenzene core resulted in a series of moderate to highly potent H₃R ligands with pK_i values between 6.01 and 8.76 as *trans* isomers (i.e., without illumination). The direct azobenzene analogue of **1**, compound **17**, bound the H₃R with only a slightly lower affinity (pK_i = 7.96 ± 0.06, Table 2) compared to **1** (pK_i = 8.29 ± 0.01, Table
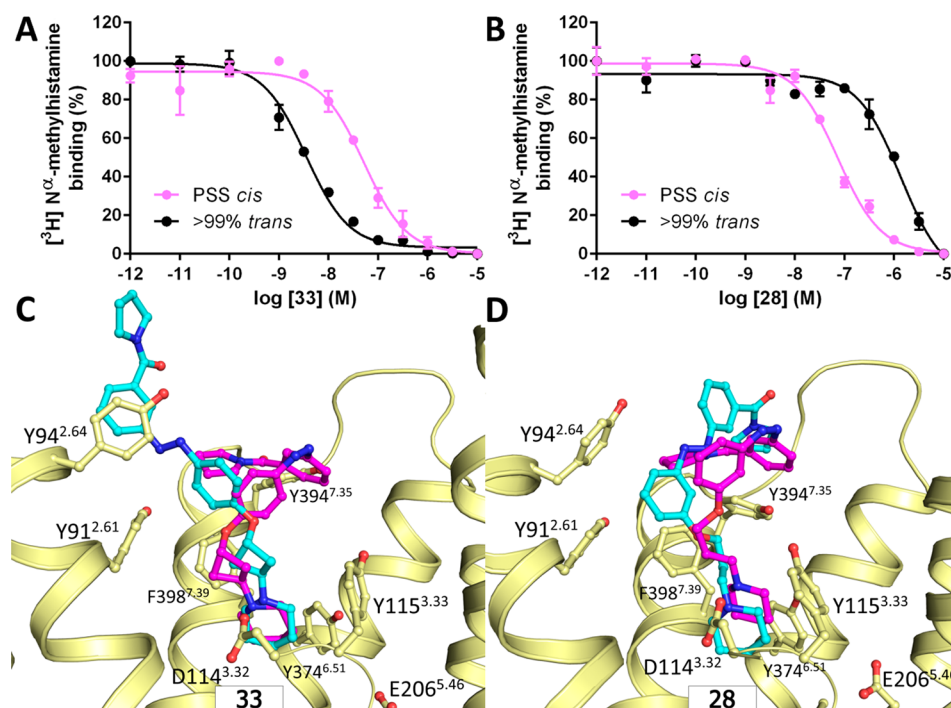
Figure 3. (A, B) Representative curves of [³H]-N$^\alpha$-methylhistamine binding displacement by increasing concentrations (A) **28** or (B) **33**. The curve indicated as PSS *cis* consists of predominantly (>90%) *cis* compound. (C, D) Proposed binding modes of (C) **28** and (D) **33** in an H₃R homology model based on representative MD snapshots. The cyan and magenta carbon atoms of the ligands correspond to the *trans* and *cis* isomer, respectively, and for the purpose of clarity, parts of ECL1/TM3 and ECL2 are not shown.

2). Furthermore, the affinity for H₃R was modulated effectively by shifting the position of the amine side chain, with scaffold A (*para*-substitution) always resulting in better affinities than scaffold B (*meta*-substitution) (Table 2). In general, the propyl spacer proved advantageous over the ethyl spacer for H₃R affinity. The effects of amide positioning varied among the different subclasses.

Rather than absolute affinities of the *trans* isomers for H₃R, the shift in affinity upon illumination was considered the prime parameter for photopharmacology applications and selection of key compounds. An increase in binding affinity upon photoisomerization (illumination at 360 ± 20 nm) was observed for **12**, **25**, **27**, **28**, and **30**. Interestingly, most of these compounds contain a *meta*-ether-substituted azobenzene core (scaffold B) with either a 3-carboxamide (**27**, **28**), a 4-carboxamide (**30**), or no carboxamide substituent (**25**). The ethyl-spaced **27** has an 8.3-fold decrease in H₃R affinity compared to the propyl-spaced analogue **28**. Within the set of compounds lacking a carboxamide, *meta*- and *para*-ether-substituted azobenzene compounds **25** and **12** (scaffolds B and A) show similar shifts in H₃R affinity upon isomerization. The 13.5-fold increase in H₃R affinity upon photoswitching of **28** (Figure 3A) led to its identification as one of the key compounds of this study (VUF14738).

Compounds that show decreased H₃R binding affinity upon isomerization were primarily found to have a *para*-ether-substituted azobenzene (scaffold A). The trend that ethyl-spaced compounds perform less well than their respective propyl-spaced analogues was also observed for the pairs **14**/**15** and **16**/**17**. Derivatives with a 2-carboxamide substituents (**13**, **26**) gave smaller shifts in H₃R affinity compared to their 3-carboxamide counterparts (**15**, **28**). The observed decreases in H₃R binding affinity upon isomerization observed for these compounds (**13**−**17**, **26**, and **29**) were deemed insufficient for

proper photopharmacological application. To address this issue, the core azobenzene-substituted scaffold was maintained, but the propyl spacer between the ether and piperidine moiety was constrained using isopropylpiperidinyl and 1,3-cyclobutyl spacers. Such linker rigidification is a known strategy to increase the binding affinity of H₃R antagonists.[33,42] Importantly, we reasoned that the limited degrees of freedom associated with the linker rigidification would hamper the *cis* isomer from (partially) readjusting its binding mode in the GPCR protein. Upon linker rigidification, the H₃R binding affinities for **31** and **33** were considerably increased compared to their flexible counterpart **15** (Table 2). Additionally, a pronounced increase in the shift in H₃R affinity between the *trans* and *cis* analogues was observed. Of note is the lower H₃R affinity of stereoisomer **32** compared to **33**, which is in accordance with previously reported data.[33] Compound **33** outperformed **31** based on having a larger shift in H₃R affinity (11.2-fold lower, Figure 3B) upon isomerization and higher absolute H₃R affinity. Moving the *trans*-cyclobutyl side chain to the *meta*-position (**34**), effectively arriving at a constrained version of key compound **28**, virtually abolished the pK_i shift and did not increase the binding affinity. All this led to the designation of **33** as the second key compound (VUF14862).

Compounds **28** and **33** either gain or lose at least 10-fold H₃R affinity upon illumination (Figure 3A,B). Thus, using the same photoswitchable core and by proper side-chain substitution in the periphery of the scaffold, we developed bidirectional GPCR photoswitchable ligands. Moreover, **28** and **33** show a 10- to 100-fold H₃R selectivity over the H₁R and no measurable affinity for H₂R and H₄R (Table S2). With the cautious use of **28** in view of its residual H₁R affinity, **28** and **33** offer a bidirectional set of photopharmacological tools for H₃R.

Binding Mode Characterization. Molecular modeling studies were performed for tool compounds **28** and **33** in order
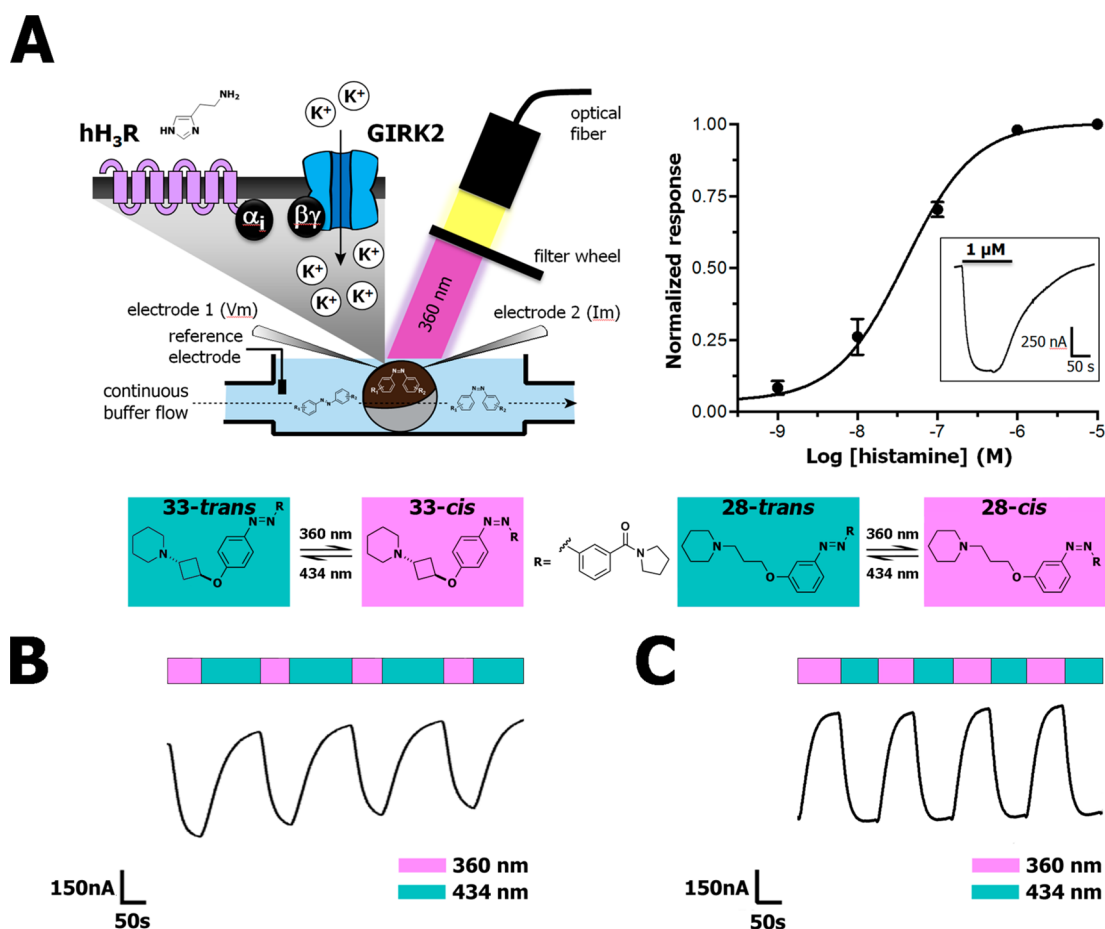
Figure 4. (A) Schematic drawing of the TEVC setup used for dynamic H_3R and GIRK current (in)activation and concentration−response curve of histamine evoked currents in *Xenopus* oocytes expressing H_3R and GIRK. The inset shows the current increase upon continuous histamine (1 μM) perfusion in time. (B) Representative part of a GIRK-mediated current trace during continuous perfusion with 5 μM histamine in competition with 1 μM **33** under illumination of the *Xenopus* oocyte with alternating 360 ± 20 and 434 ± 9 nm wavelength as measured by TEVC. An extended time trace is available in Figure S34. (C) Representative part of a GIRK-mediated current trace during continuous perfusion with 5 μM histamine in competition with 1 μM **28** and illumination of the oocyte with alternating 360 ± 20 and 434 ± 9 nm wavelength as measured by TEVC. An extended time trace is available in Figure S35.

to gain insights into the molecular mechanism of the observed affinity changes upon isomerization. Molecular docking of **28** and **33** into a series of H_3R homology models yielded three potential binding modes in which the ligands form either an ionic interaction with the $D114^{3.32}$ or $E206^{5.46}$ residue in transmembrane helices (TM) 3 and 5, respectively.[24,43,44] The predicted binding modes share similarity with the binding orientation of ergotamine as observed in crystal structures of serotonin receptors 5-HT$_{1B}$ and 5-HT$_{2B}$ (PDB IDs: 4IAR, 4IB4),[45,46] aminergic GPCRs that share 54−62% sequence similarity for the binding site with H_3R (Figure S22). Each of the 12 resulting H_3R−ligand complexes (2 ligands × 2 isomers × 3 binding modes) was investigated using 50 ns molecular dynamics (MD) simulations. The MD trajectories indicated that only for one binding mode (Figure S22A) (i) a consistent interaction fingerprint (IFP)[47] was observed throughout the simulation and (ii) the stable ligand binding mode was in line with the observed SAR data (Table 2). In this binding mode (Figure 3C,D) the ligands form a stable salt bridge with $D114^{3.32}$ and move upward along TMs 2, 3, and 7 into the extracellular vestibule (ECV). The *trans* isomer of **33** adopts an elongated binding mode and makes multiple aromatic stacking interactions with $Y91^{2.61}$, $Y94^{2.64}$, $Y394^{7.35}$, and $F398^{7.39}$, while

the carboxamide substituent is solvent exposed between the extracellular loops 1 and 2 (Figure 3D). The *trans* isomer of **28**, on the other hand, adopts an arched binding mode within the extracellular vestibule (Figure 3C) due to its *meta*-substitution. The binding modes of the *trans* isomers of both **28** and **33** are similar to the previously proposed binding modes for bitopic ligands of the aminergic dopamine D_2 receptor.[48] The *cis* isomers of both **28** and **33** adopt an almost identical binding mode (Figure 3C,D) in which the carboxamide is buried in the ECV in close proximity to $Y394^{7.35}$, folded against the azobenzene, and located at the same position as the pyrrolidine moiety of ergotamine bound to 5-HT$_{1B}$ and 5-HT$_{2B}$ crystal structures (Figure S23).

The opposite effects of *trans* to *cis* isomerization on the H_3R binding affinities of **28** and **33** can be explained by differences in (i) the complementarity of polar or apolar surface areas of the ligand and the protein binding site[49] and (ii) the loss of conformational degrees of freedom as the result of ligand binding (conformer focusing[50]). Both isomers of **33** are expected to be less affected by conformer focusing due to their rigid cyclobutyl-spacer compared to the flexible propyl spacer of **28**. The decreased affinity of the *trans* isomer versus the *cis* isomer of **28** (Table 2) can be explained by the fact that

the apolar surface area of **28** is >4 times more solvent exposed in the *trans* isomer binding mode than in the *cis* isomer binding mode in H$_3$R. Conversely, the *trans* isomer of **33** has a reduced buried polar surface area compared to the folded *cis* isomer, while the apolar surface area of **33** is able to form a complementary fit with the apolar surface area of the H$_3$R binding site. In addition, the extended *trans* isomer of **33** allows more degrees of conformational freedom than the folded *cis* isomer, altogether resulting in an increased H$_3$R affinity for the *trans* isomer of **33** (Table 2).

Dynamic Photochemical Modulation of H$_3$R. As the new azobenzene-containing H$_3$R photoswitches can be dynamically and reversibly isomerized with light, we applied the two key H$_3$R photoswitches in a dynamic intact cell system with a real-time readout. Two-electrode voltage clamp (TEVC) using *Xenopus laevis* oocytes co-expressing H$_3$R and a GIRK channel composed of human GIRK1 (Kir3.1) and GIRK4 (Kir3.4) subunits (Figure 4A)[51] allows for a real-time H$_3$R readout. In all experiments, H$_3$R-expressing oocytes were used that evoked a high current (>500 nA) upon histamine superfusion in 64 mM NaCl, 25 mM KCl, 15 mM HEPES, 0.8 mM MgCl$_2$, and 0.4 mM CaCl$_2$ pH 7.4 at a membrane potential of −80 mV. Under these conditions, histamine induced GIRK channel activation with a pEC$_{50}$ value of 7.3 ± 0.06 (Figure 4A). No currents were observed after histamine application to noninjected oocytes (Figure S24). The GIRK channel activation by histamine (1 μM) could be fully inhibited upon simultaneous superfusion with the H$_3$R antagonist clobenpropit (1 μM) or by pretreating the oocytes with the Gα$_i$-protein inhibitor pertussis toxin (1.37 ng/oocyte) (Figures S25 and S26). This shows that the histamine-induced current in *Xenopus laevis* oocytes coexpressing H$_3$R and a GIRK channel composed of human GIRK1 (Kir3.1) and GIRK4 (Kir3.4) subunits is H$_3$R mediated through G$_i$-protein coupling to GIRK.

We first ensured that photoisomerization behavior of **28** and **33** in HEPES pH 7.4 buffer was similar to behavior in 50 mM Tris−HCl pH 7.4 buffer (Figure S4−S15). Next, we superfused *Xenopus* oocytes expressing H$_3$R and a GIRK channel with histamine and either *trans*-**28** or *trans*-**33** for dynamic receptor inhibition studies. Superfusion of only **28** or **33** on both noninjected and H$_3$R-GIRK expressing oocytes did not result in changes in current, confirming that these H$_3$R ligands act as antagonists (Figure S27−S30). Illumination directly on the oocytes (Figure 4A) in the absence of **28** or **33** did not change the magnitude of histamine evoked currents (Figure S31). Yet, in the presence of either **33** or **28**, clear photoswitchable antagonism of the histamine-induced current was observed under alternating illumination. We confirmed that both compounds were able to show this behavior in a concentration-dependent fashion (Figures S32 and S33), yielding K_i values for **33** that nicely match the K_i values obtained in the radioligand binding experiments (TEVC pK_i > 99% *trans*: 8.72 ± 0.11, PSS *cis*: 7.98 ± 0.15, radioligand binding: pK_i > 99% *trans*: 8.76 ± 0.09, PSS *cis*: 7.71 ± 0.09). An increase in histamine-induced GIRK activation was observed when *trans*-**33** was illuminated with 360 ± 20 nm, confirming that the H$_3$R antagonistic effect of **33** is reduced upon isomerization to its *cis* isomer. When subsequently the superfused oocytes were illuminated at 434 ± 9 nm, a decrease in H$_3$R-induced GIRK activation was observed due to a stronger H$_3$R antagonistic effect by the *trans* isomer of **33** as a consequence of increased H$_3$R binding affinity. This effect could be repeated several times

in subsequent illumination cycles in the same experiment (Figure 4B). For **28**, the reciprocal light-induced H$_3$R affinity shift compared to **33** translated well to a reciprocal effect upon illumination in the TEVC setup (Figure 4C). That is, **28** reached the highest H$_3$R inhibition, measured as reduced histamine-induced GIRK channel activation, upon illumination with 360 ± 20 nm. Also, **28** could be effectively switched back in the TEVC setup upon illumination with 434 ± 9 nm, and again the GPCR blocking properties could be modulated by alternating illumination (Figure 4C). These experiments demonstrate the rapid bidirectional modulation of the H$_3$R using the two complementary photoswitchable ligands **28** and **33**.

CONCLUSIONS

A robust bidirectional photochemical toolbox for dynamic antagonism of the H$_3$R has been successfully developed using a core-centered approach replacing a naphthalene moiety in a known scaffold by a properly substituted azobenzene unit. SAR exploration delivered 16 compounds that show a shift in binding affinity for the H$_3$R upon photoisomerization. Two key compounds, **28** and **33**, were selected on the basis of their 13.5-fold increase or 11.2-fold decrease in H$_3$R binding affinity upon photoisomerization, respectively. The long thermal relaxation half-lives and resistance to fatigue of these compounds allowed in-depth spectroscopic analysis (NMR, LC−MS, UV−vis) of the photochemical properties. The rapid photochemical isomerization directly translated to dynamic, light-modulated H$_3$R blockade in real-time electrophysiology experiments using H$_3$R and GIRK coexpressing *Xenopus* oocytes. In this dynamic experimental setup, histamine-induced GPCR activation could be modulated on a time scale of seconds, and we were able to show real-time, light-sensitive blockade of the H$_3$R activation by both new tool compounds. In our view, **28** (VUF14738) and **33** (VUF14862) are highly useful photopharmacological tools for temporal studies to dissect the complex signaling cascade of H$_3$R. Moreover, the presented bidirectional modulation of H$_3$R protein by closely related photosensitive analogs of the same core scaffold further emphasizes the exceptional opportunities of conformational modulation of the GPCR protein family.

EXPERIMENTAL SECTION

Synthesis and Characterization of Compounds. All starting materials were obtained from commercial suppliers (primarily being Sigma-Aldrich, Acros Organics, Fluorochem, and Strem Chemicals) and used without purification. 4-Hydroxyazobenzene (**8**) was obtained from Sigma-Aldrich. *cis*-3-Piperidin-1-ylcyclobutanol (**35**) was synthesized according to the literature procedure of Wijtmans et al.[33] Anhydrous THF and DCM were obtained by passing them through an activated alumina column prior to use. Anhydrous toluene was freshly distilled over CaH$_2$ or dried over activated 4 Å molecular sieves, which were added at least 24 h before use. Anhydrous DMF was purchased from Acros Organics (Geel, Belgium) and used without prior purification. All reactions were carried out under nitrogen atmosphere unless mentioned otherwise. TLC analyses were performed using Merck F254 aluminum-backed silica plates and visualized with 254 nm UV light or a potassium permanganate stain. Flash column chromatography was executed using Silicycle Siliaflash F60 silica gel or by means of a Biotage Isolera equipment using Biotage SNAP columns. All HRMS spectra were recorded on a Bruker micrOTOF mass spectrometer using ESI in positive-ion mode. All NMR spectra were recorded on either a Bruker Avance 250, Bruker Avance 400, Bruker Avance 500, or Bruker Avance 600 spectrometer. The peak multiplicities are defined as follows: s, singlet; d, doublet; t, triplet; q, quartet; p, pentet; dd, doublet of doublets; dt, doublet of triplets; td,

triplet of doublets; bs, broad singlet; m, multiplet. The spectra were referenced to the internal solvent peak as follows: $CDCl_3$ (^1H = 7.26 ppm, ^{13}C = 77.16 ppm), DMSO-d_6 (^1H = 2.50 ppm, ^{13}C = 39.52 ppm), CD_3OD (^1H = 3.31 ppm, ^{13}C = 49.00 ppm).[52] IUPAC names were adapted from ChemBioDraw Ultra 14.0 (PerkinElmer). Purities were measured with the aid of analytical LC−MS using a Shimadzu LC-20AD liquid chromatography pump system with a Shimadzu SPDM20A diode array detector with the MS detection performed with a Shimadzu LCMS-2010EV mass spectrometer operating in both positive and negative ionization mode. The column used was an Xbridge (C18) 5 μm column (50 mm × 4.6 mm or 100 mm × 4.6 mm). The following solutions are used for the eluents. Solvent A: water/formic acid 999:1 and solvent B: acetonitrile/formic acid 999:1. The eluent program used is as follows: flow rate: 1.0 mL/min, start 95% A in a linear gradient to 10% A over 4.5 min, hold 1.5 min at 10% A, in 0.5 min in a linear gradient to 95% A, hold 1.5 min at 95% A, total run time: 8.0 min. Compound purities were calculated as the percentage peak area of the analyzed compound by UV detection at 254 nm. All chemistry and analyses of photosensitive compounds were carried out under dimmed or red light.

Detailed chemical experimental procedures and chemical analyses are supplied in the Supporting Information.

Photochemistry. UV−vis spectra were obtained using a Thermo-scientific Evolution 201 PC spectrophotometer or a Shimadzu UV-2401 PC spectrophotometer. Fits of UV−vis spectroscopy data were generated using Mathworks Matlab R2014A (8.3.0.532). Illumination was executed using a Sutter instruments Lambda LS with a 300 W full-spectrum lamp connected to a Sutter instruments Lambda 10-3 optical filter changer equipped with 434 ± 9 nm and 360 ± 20 nm filters. For photochemical analyses illuminations were performed in Hellma Suprasil quartz 114-QS cuvettes. Thermal relaxation experiments and Arrhenius extrapolations were performed according to Priimagi et al.[34] using a compound concentration of 25 μM in 50 mM Tris−HCl pH 7.4 buffer +1% DMSO-d_6 and temperatures of 60, 70, and 80 °C. Illuminations for pharmacological experiments were performed in cylindrical clear glass vials with a volume of 4.5 mL. The typical distance between light source and vial or cuvette was 2 cm. In illuminations during TVEC experiments the light-source was positioned at 5 cm from the chamber containing the oocyte. The focused beam of the light source has a diameter of 1.8 cm and the beam was pointed such that it illuminated the full oocyte. The light intensity on the oocyte is 0.77 mW/mm^2 using the 360 ± 20 nm filter and 0.57 mW/mm^2 for the 434 ± 9 nm filter as measured using a Thorlabs PM16−401 power meter.

Computational Chemistry. *Homology Model Construction.* The sequence of H_3R was obtained from UniProt (accession code Q9Y5N1) and aligned to the unique sequences of crystallized aminergic GPCRs (PDB accessed at 3 Nov 2015). The sequence similarity and identity were assessed for the full sequence, each TM helix, extracellular loop 2, and the binding pocket as previously defined.[23] On the basis of this analysis, the sequence alignment of H_3R to H_1R, M_3R, D_3R, 5-$HT_{1B}R$, and 5-$HT_{2B}R$ and their crystal structures (PDB codes 3RZE, 4U15, 3PBL, 4IAR, and 4IB4) were used as input for MODELER (version 9.15).[53] Five hundred different homology models were constructed from which 36 were selected based on visual inspection. Compounds *trans*-**28**, *cis*-**28**, *trans*-**33**, and *cis*-**33** were subsequently docked into each model using PLANTS[54] (settings: speed 1, scoring function ChemPLP, 10-fold docking, 50 proposed poses per fold) into each of the models while treating the side chains of E206$^{5.46}$ and F398$^{7.39}$ as flexible. The resulting 26000 docking poses were filtered using IFP[47] on either and ionic and H-bond interaction with D114$^{3.32}$ or E206$^{5.46}$ from which the top 5 ChemPLP-scored poses were kept for further processing, yielding 396 H_3R−ligand complexes. Visual inspection highlighted three clusters of potential binding modes. From each ligand in each binding mode cluster one model was selected for further investigation with molecular dynamics simulations.

Molecular Dynamics Simulations. Each ligand−H_3R complex was aligned to the membrane-aligned H_1R structure from the OPM database. A sodium ion was added in the sodium binding site based on high-resolution sodium-bound β_1-adrenoceptor crystal structure (PDB code 4BVN). Subsequently, the rotamers from the sodium binding site residues were manually optimized.[55] The H_3R−ligand complexes were embedded in a pre-equilibrated box containing a lipid bilayer (134 POPC lipids), explicit solvent (∼11000 water molecules), and a 0.15 M concentration of NaCl (∼70 ions). Using MOE (v2015.1001; Chemical Computing Group, Inc., Montreal, Quebec, Canada), the ligand−H_3R complex was solvated, and waters between the receptor and the membrane and outside the receptor were removed. The ligands were parametrized for GAFF using Amber's antechamber with AM1-BCC partial charges. The resulting parameters of the ligand were checked, and the azobenzene parameters were optimized in line with the parameters reported by Schäfer et al.[56] The AMBER99SB*-ILDN force field was used for the protein and the lipids and waters were described according to the Berger lipid parameters and the TIP3P model, respectively.[57] After the system was neutralized, a 1000-step steepest descent minimization of the system was performed after which the complex was equilibrated for 75 and 300 ps using a 1 and 2 fs time step, respectively. A subsequent production run of 50 ns as an NVT ensemble was performed for each combination. The trajectories were analyzed using IFP[47] resulting in a time-based interaction profile for each H_3R−ligand complex. These MD simulations were performed using GROMACS 5.1.[58]

Pharmacology. *General Data.* Within this paper, the 445-isoform of the human H_3R is referred to as wild-type receptor. [^3H]-Mepyramine (specific activity 20 Ci/mmol^{-1}), [^{125}I]-iodoaminopotentidine (specific activity 2200 Ci/mmol^{-1}), [^3H]-N^α-methylhist-amine (specific activity 78.3 Ci/mmol^{-1}), and [^3H]-histamine (specific activity 17.5 Ci/mmol^{-1}) were purchased from PerkinElmer (Groningen, The Netherlands). All other chemicals were of analytical grade and obtained from commercial sources.

Cell Culture and Transfection. Human embryonic kidney 293T cells (HEK293T cells) were cultured in Dulbecco's modified eagle medium (DMEM) supplemented with 10% fetal bovine serum (FBS), penicillin (50 IU/mL), and streptomycin (50 μg/mL). HEK293T cells were transiently transfected with H_3R cDNA using the polyethylenimine (PEI) method. In brief, 24 h prior to transfection 2 × 10^6 cells were seeded on a 10 cm dish. Cells were transfected with 5 μg of H_3R cDNA and 20 μg of PEI in 500 μL of 150 mM NaCl solution. The DNA−PEI mixture was incubated for 15−30 min at 22 °C before dropwise addition to the cells. Cells were maintained for 48 h at 37 °C with 5% CO_2 before harvesting.

Preparation of Cell Homogenates. Forty-eight hours after transfection, cells were detached and collected from the plates by vigorous pipetting using phosphate-buffered saline (PBS). Cells were centrifuged at 3000 rpm for 10 min, and the cell-pellet was stored at −20 °C until the day of the experiment.

Radioligand-Binding Assay. For radioligand binding experiments, samples were pretreated to obtain *trans* and *cis* samples. In brief, a 1 mM ligand solution was divided in two samples which were either illuminated at 360 ± 20 nm until their photostationary state was reached as analyzed by LC−MS or kept in the dark for the same duration as the illuminated samples. All subsequent handling was performed in the dark or under near-infrared light. [^3H]-N^α-Methylhistamine binding assays were performed in a total volume of 100 μL consisting of cold ligand (increasing concentration ranging from 10^{-5} to 10^{-12} M) prepared in assay buffer [50 mM Tris−HCl pH 7.4], 1.6 nM [^3H]-N^α-methylhistamine, and HEK293T cell homogenates transiently expressing the human H_3R (>25 μg/50 μL). The mixture was incubated for 2 h at 25 °C before termination by rapid filtration over a 96 well GF/C filter plate precoated with 0.5% PEI using PerkinElmer 96-well filtermate-harvester (PerkinElmer). The filter was washed five times with ice-cold wash buffer [50 mM Tris-HCl pH 7.4, 4 °C]. Five hours after addition of Microscint O scintillation liquid, filter-bound radioactivity was measured using a microbeta wallac trilux scintillation counter (PerkinElmer).

Binding Selectivity Screening. H_1R radioligand binding assays were performed according to the method of Kuhne et al.[59] using an incubation time of 2 h instead of 4 h. H_2R radioligand binding assays were performed according to Leurs et al.[60] using HEK293T cells

instead of CHO cells and a total volume of 400 μL instead of 200 μL. H_4R radioligand binding assays were performed according to the method of Nijmeijer et al.[61]

Data Analysis. All experiments were analyzed using Graphpad prism 6.05 (Graphpad Software, Inc., San Diego, CA). IC_{50} values obtained from competition binding experiments were converted to K_i values using the Cheng−Prusoff equation.[62]

Two-Electrode Voltage Clamp Assay. *cRNA Synthesis.* The Kir3.1 and Kir3.4 were both supplied in the pcDNA3.1 vector and were a kind gift of K. Sahlholm (Karolinska Institute, Stockholm, Sweden). The H_3R was cloned into the pCIneo vector. Restriction enzymes BAMHI and NdeI were used to linearize the constructs pCIneo-H_3R and pcDNA3.1-Kir3.1 and 3.4, respectively. After the digestion, 0.5% SDS and Proteinase K (200 μg/mL) were added, and the mixture was incubated at 50 °C for 30 min. DNA was extracted by phenol/chloroform and the precipitation method. The quality and digestion were checked on 1% agarose gel. The cRNA synthesis was performed with the T7 mMessage mMachine kit (Ambion, Austin, TX). After the synthesis, the cRNA quality and amount were checked on a denaturing gel for RNA as described by Almeida et al.[63]

H_3R and GIRK Expression in Oocytes. *Xenopus laevis* oocytes were supplied as "topgrade" oocytes (Ecocyte, Castrop-Rauxel, Germany). Each oocyte was injected with a volume of 46 nL, containing 3 ng cRNA of each GIRK subunit and 50 ng cRNA of the H_3R or with 46 nL of RNase free water as control with the Nanoject II (Drummond Scientific Company, Broomall, PA). The oocytes were incubated for 4−6 days at 12 °C in modified Barth solution (88 mM NaCl, 1 mM KCl, 2.4 mM $NaHCO_3$, 15 mM HEPES, 0.33 mM $Ca(NO_3)_2$, 0.41 mM $CaCl_2$, 0.82 mM $MgSO_4$, 2.5 mg pyruvic acid, 100 μg/mL streptomycin, 50 μg/mL gentamycin, adjusted with Tris to pH 7.4), as described by Sahlholm et al.[51]

Two-Electrode Voltage Clamp. TEVC was performed with an Axoclamp 900A amplifier and a Digidata 1550 Digitizer. The currents were recorded and analyzed with pClamp 10.6 (Molecular Devices, Sunnyvale, CA). Glass micropipettes were pulled from borosilicate capillaries (GC150-10, Harvard Apparatus, Edenbridge, UK) with the P-1000 micropipette puller (Sutter Instrument, Novato, CA) to have a resistance of 1−3 MΩ when filled with 3 M KCl solution. The oocyte was positioned in the recording chamber (RC-1Z, Warner Instruments, Hamden, CT), and by gravity flow, high potassium solution (64 mM NaCl, 25 mM KCl, 0.8 mM $MgCl_2$, 0.4 mM $CaCl_2$, 15 mM HEPES and adjusted with Bis-Tris Propane to pH 7.4) was perfused through the recording chamber. For the study of H_3R ligands, the membrane potential was clamped at −80 mV and the evoked currents were measured at room temperature (~20 °C). The ligands (histamine, clobenpropit, **28** and **33**) were diluted in the high potassium solution to obtain the appropriate concentrations. For the photoswitchable ligands (**28** and **33**), the TEVC was performed in the dark, and the different wavelengths (360 ± 20 nm and 434 ± 9 nm) were applied directly on the oocyte in the recording chamber for 1 min (with **28**) or 2 min (with **33**) with a Sutter instruments Lambda LS with a 300 W full spectrum lamp connected to a Sutter instruments Lambda 10−3 optical filter changer equipped with 434 ± 9 nm and 360 ± 20 nm filters to observe the (functional) switch of the ligands. For the pertussis toxin experiment, 46 nL (1.38 ng) of PTX or water as control was injected in H_3R/GIRK expressing oocytes (4−6 days after cRNA injection) with the Nanoject II The oocytes were incubated for another 7 h before measuring the currents evoked by 1 μM histamine to the oocytes.

ASSOCIATED CONTENT

Ⓢ Supporting Information

The Supporting Information is available free of charge on the ACS Publications website at DOI: 10.1021/jacs.7b11422.

Detailed synthetic procedures, chemical analyses and spectra, and additional data as noted in the text (PDF)

AUTHOR INFORMATION

Corresponding Authors
*m.wijtmans@vu.nl
*r.leurs@vu.nl

ORCID 🟢

Chris De Graaf: 0000-0002-1226-2150
Rob Leurs: 0000-0003-1354-2848

Notes
The authors declare no competing financial interest.

REFERENCES

(1) Broichhagen, J.; Frank, J. A.; Trauner, D. *Acc. Chem. Res.* **2015**, *48*, 1947.
(2) Lerch, M. M.; Hansen, M. J.; van Dam, G. M.; Szymanski, W.; Feringa, B. L. *Angew. Chem., Int. Ed.* **2016**, *55*, 10978.
(3) Szobota, S.; Isacoff, E. Y. *Annu. Rev. Biophys.* **2010**, *39*, 329.
(4) Beharry, A. A.; Woolley, G. A. *Chem. Soc. Rev.* **2011**, *40*, 4422.
(5) Szymanski, W.; Beierle, J. M.; Kistemaker, H. A.; Velema, W. A.; Feringa, B. L. *Chem. Rev.* **2013**, *113*, 6114.
(6) Velema, W. A.; Szymanski, W.; Feringa, B. L. *J. Am. Chem. Soc.* **2014**, *136*, 2178.
(7) Stein, M.; Middendorp, S. J.; Carta, V.; Pejo, E.; Raines, D. E.; Forman, S. A.; Sigel, E.; Trauner, D. *Angew. Chem., Int. Ed.* **2012**, *51*, 10500.
(8) Frank, J. A.; Moroni, M.; Moshourab, R.; Sumser, M.; Lewin, G. R.; Trauner, D. *Nat. Commun.* **2015**, *6*, 7118.
(9) Broichhagen, J.; Schonberger, M.; Cork, S. C.; Frank, J. A.; Marchetti, P.; Bugliani, M.; Shapiro, A. M.; Trapp, S.; Rutter, G. A.; Hodson, D. J.; Trauner, D. *Nat. Commun.* **2014**, *5*, 5116.
(10) Pittolo, S.; Gomez-Santacana, X.; Eckelt, K.; Rovira, X.; Dalton, J.; Goudet, C.; Pin, J. P.; Llobet, A.; Giraldo, J.; Llebaria, A.; Gorostiza, P. *Nat. Chem. Biol.* **2014**, *10*, 813.
(11) Schönberger, M.; Trauner, D. *Angew. Chem., Int. Ed.* **2014**, *53*, 3264.
(12) Bahamonde, M. I.; Taura, J.; Paoletta, S.; Gakh, A. A.; Chakraborty, S.; Hernando, J.; Fernandez-Duenas, V.; Jacobson, K. A.; Gorostiza, P.; Ciruela, F. *Bioconjugate Chem.* **2014**, *25*, 1847.
(13) Broichhagen, J.; Johnston, N. R.; von Ohlen, Y.; Meyer-Berg, H.; Jones, B. J.; Bloom, S. R.; Rutter, G. A.; Trauner, D.; Hodson, D. J. *Angew. Chem., Int. Ed.* **2016**, *55*, 5865.
(14) Westphal, M.; Schafroth, M. A.; Sarott, R.; Imhof, M.; Bold, C.; Leippe, P.; Dhopeshwarkar, A.; Grandner, J.; Katritch, V.; Mackie, K.; Trauner, D.; Carreira, E. M.; Frank, J. A. *J. Am. Chem. Soc.* **2017**, *139*, 18206.
(15) Haas, H.; Panula, P. *Nat. Rev. Neurosci.* **2003**, *4*, 121.
(16) Leurs, R.; Bakker, R. A.; Timmerman, H.; de Esch, I. J. P. *Nat. Rev. Drug Discovery* **2005**, *4*, 107.

(17) Panula, P.; Chazot, P. L.; Cowart, M.; Gutzmer, R.; Leurs, R.; Liu, W. L.; Stark, H.; Thurmond, R. L.; Haas, H. L. *Pharmacol. Rev.* **2015**, *67*, 601.

(18) Schwartz, J. C. *Br. J. Pharmacol.* **2011**, *163*, 713.

(19) Lebois, E. P.; Jones, C. K.; Lindsley, C. W. *Curr. Top. Med. Chem.* **2011**, *11*, 648.

(20) Leurs, R.; Vischer, H. F.; Wijtmans, M.; de Esch, I. J. P. *Trends Pharmacol. Sci.* **2011**, *32*, 250.

(21) Celanire, S.; Wijtmans, M.; Talaga, P.; Leurs, R.; de Esch, I. J. *Drug Discovery Today* **2005**, *10*, 1613.

(22) Uveges, A. J.; Kowal, D.; Zhang, Y.; Spangler, T. B.; Dunlop, J.; Semus, S.; Jones, P. G. *J. Pharmacol. Exp. Ther.* **2002**, *301*, 451.

(23) Kooistra, A. J.; Kuhne, S.; de Esch, I. J.; Leurs, R.; de Graaf, C. *Br. J. Pharmacol.* **2013**, *170*, 101.

(24) Axe, F. U.; Bembenek, S. D.; Szalma, S. *J. Mol. Graphics Modell.* **2006**, *24*, 456.

(25) Lorenzi, S.; Mor, M.; Bordi, F.; Rivara, S.; Rivara, M.; Morini, G.; Bertoni, S.; Ballabeni, V.; Barocelli, E.; Plazzi, P. V. *Bioorg. Med. Chem.* **2005**, *13*, 5647.

(26) Kim, S.-K.; Fristrup, P.; Abrol, R.; Goddard, W. A. *J. Chem. Inf. Model.* **2011**, *51*, 3262.

(27) Sander, K.; von Coburg, Y.; Camelin, J. C.; Ligneau, X.; Rau, O.; Schubert-Zsilavecz, M.; Schwartz, J. C.; Stark, H. *Bioorg. Med. Chem. Lett.* **2010**, *20*, 1581.

(28) Roche, O.; Nettekoven, M.; Vifian, W.; Sarmiento, R. M. *Bioorg. Med. Chem. Lett.* **2008**, *18*, 4377.

(29) Arrang, J. M.; Garbarg, M.; Lancelo, J. C.; Lecomte, J. M.; Pollard, H.; Robba, M.; Schunack, W.; Schwartz, J. C. *Nature* **1987**, *327*, 117.

(30) Alves-Rodrigues, A.; Leurs, R.; Wu, T. S.; Prell, G. D.; Foged, C.; Timmerman, H. *Br. J. Pharmacol.* **1996**, *118*, 2045.

(31) Nieto-Alamilla, G.; Marquez-Gomez, R.; Garcia-Galvez, A. M.; Morales-Figueroa, G. E.; Arias-Montano, J. A. *Mol. Pharmacol.* **2016**, *90*, 649.

(32) Wu, X.; Fors, B. P.; Buchwald, S. L. *Angew. Chem., Int. Ed.* **2011**, *50*, 9943.

(33) Wijtmans, M.; Denonne, F.; Celanire, S.; Gillard, M.; Hulscher, S.; Delaunoy, C.; Van Houtvin, N.; Bakker, R. A.; Defays, S.; Gerard, J.; Grooters, L.; Hubert, D.; Timmerman, H.; Leurs, R.; Talaga, P.; de Esch, I. J. P.; Provins, L. *MedChemComm* **2010**, *1*, 39.

(34) Ahmed, Z.; Siiskonen, A.; Virkki, M.; Priimagi, A. *Chem. Commun.* **2017**, *53*, 12520.

(35) Bleger, D.; Hecht, S. *Angew. Chem., Int. Ed.* **2015**, *54*, 11338.

(36) Dong, M.; Babalhavaeji, A.; Hansen, M. J.; Kalman, L.; Woolley, G. A. *Chem. Commun. (Cambridge, U. K.)* **2015**, *51*, 12981.

(37) Talaty, E. R.; Fargo, J. C. *Chem. Commun.* **1967**, *0*, 65.

(38) Garcia-Amoros, J.; Velasco, D. *Beilstein J. Org. Chem.* **2012**, *8*, 1003.

(39) Asano, T.; Okada, T.; Shinkai, S.; Shigematsu, K.; Kusano, Y.; Manabe, O. *J. Am. Chem. Soc.* **1981**, *103*, 5161.

(40) Serra, F.; Terentjev, E. M. *Macromolecules* **2008**, *41*, 981.

(41) Whitten, D. G.; Wildes, P. D.; Pacifici, J. G.; Irick, G. *J. Am. Chem. Soc.* **1971**, *93*, 2004.

(42) Dvorak, C. A.; Apodaca, R.; Barbier, A. J.; Berridge, C. W.; Wilson, S. J.; Boggs, J. D.; Xiao, W.; Lovenberg, T. W.; Carruthers, N. I. *J. Med. Chem.* **2005**, *48*, 2229.

(43) Rai, B. K.; Tawa, G. J.; Katz, A. H.; Humblet, C. *Proteins: Struct., Funct., Genet.* **2010**, *78*, 457.

(44) Levoin, N.; Labeeuw, O.; Krief, S.; Calmels, T.; Poupardin-Olivier, O.; Berrebi-Bertrand, I.; Lecomte, J. M.; Schwartz, J. C.; Capet, M. *Bioorg. Med. Chem.* **2013**, *21*, 4526.

(45) Wang, C.; Jiang, Y.; Ma, J.; Wu, H.; Wacker, D.; Katritch, V.; Han, G. W.; Liu, W.; Huang, X. P.; Vardy, E.; McCorvy, J. D.; Gao, X.; Zhou, X. E.; Melcher, K.; Zhang, C.; Bai, F.; Yang, H.; Yang, L.; Jiang, H.; Roth, B. L.; Cherezov, V.; Stevens, R. C.; Xu, H. E. *Science* **2013**, *340*, 610.

(46) Wacker, D.; Wang, C.; Katritch, V.; Han, G. W.; Huang, X. P.; Vardy, E.; McCorvy, J. D.; Jiang, Y.; Chu, M.; Siu, F. Y.; Liu, W.; Xu, H. E.; Cherezov, V.; Roth, B. L.; Stevens, R. C. *Science* **2013**, *340*, 615.

(47) Marcou, G.; Rognan, D. *J. Chem. Inf. Model.* **2007**, *47*, 195.

(48) Lane, J. R.; Donthamsetti, P.; Shonberg, J.; Draper-Joyce, C. J.; Dentry, S.; Michino, M.; Shi, L.; Lopez, L.; Scammells, P. J.; Capuano, B.; Sexton, P. M.; Javitch, J. A.; Christopoulos, A. *Nat. Chem. Biol.* **2014**, *10*, 745.

(49) Schmidtke, P.; Luque, F. J.; Murray, J. B.; Barril, X. *J. Am. Chem. Soc.* **2011**, *133*, 18903.

(50) Tirado-Rives, J.; Jorgensen, W. L. *J. Med. Chem.* **2006**, *49*, 5880.

(51) Sahlholm, K.; Nilsson, J.; Marcellino, D.; Fuxe, K.; Arhem, P. *Eur. J. Pharmacol.* **2007**, *567*, 206.

(52) Fulmer, G. R.; Miller, A. J. M.; Sherden, N. H.; Gottlieb, H. E.; Nudelman, A.; Stoltz, B. M.; Bercaw, J. E.; Goldberg, K. I. *Organometallics* **2010**, *29*, 2176.

(53) Sali, A.; Blundell, T. L. *J. Mol. Biol.* **1993**, *234*, 779.

(54) Korb, O.; Stutzle, T.; Exner, T. E. *J. Chem. Inf. Model.* **2009**, *49*, 84.

(55) Miller-Gallacher, J. L.; Nehme, R.; Warne, T.; Edwards, P. C.; Schertler, G. F.; Leslie, A. G.; Tate, C. G. *PLoS One* **2014**, *9*, No. e92727.

(56) Schäfer, L. V.; Muller, E. M.; Gaub, H. E.; Grubmuller, H. *Angew. Chem., Int. Ed.* **2007**, *46*, 2232.

(57) Cordomi, A.; Caltabiano, G.; Pardo, L. *J. Chem. Theory Comput.* **2012**, *8*, 948.

(58) Berendsen, H. J. C.; van der Spoel, D.; van Drunen, R. *Comput. Phys. Commun.* **1995**, *91*, 43.

(59) Kuhne, S.; Kooistra, A. J.; Bosma, R.; Bortolato, A.; Wijtmans, M.; Vischer, H. F.; Mason, J. S.; de Graaf, C.; de Esch, I. J.; Leurs, R. *J. Med. Chem.* **2016**, *59*, 9047.

(60) Leurs, R.; Smit, M. J.; Menge, W. M.; Timmerman, H. *Br. J. Pharmacol.* **1994**, *112*, 847.

(61) Nijmeijer, S.; Vischer, H. F.; Rosethorne, E. M.; Charlton, S. J.; Leurs, R. *Mol. Pharmacol.* **2012**, *82*, 1174.

(62) Cheng, Y.-C.; Prusoff, W. H. *Biochem. Pharmacol.* **1973**, *22*, 3099.

(63) Almeida, P.; de Boer, G.-J.; de Boer, A. H. *J. Plant Physiol.* **2014**, *171*, 438.